Self-organized superconducting textures in thin films

Andreas Glatz,[1] Igor S. Aranson,[1] Tatyana I. Baturina,[1,2] Nikolay M. Chtchelkatchev,[1,3,4,5] and Valerii M. Vinokur[1]

[1]*Materials Science Division, Argonne National Laboratory, Argonne, Illinois 60439, USA*

[2]*A. V. Rzhanov Institute of Semiconductor Physics SB RAS, 13 Lavrentjev Avenue, Novosibirsk 630090, Russia*

[3]*Institute for High Pressure Physics, Russian Academy of Sciences, Troitsk 142190, Moscow Region, Russia*

[4]*Department of Theoretical Physics, Moscow Institute of Physics and Technology, 141700 Moscow, Russia*

[5]*L.D. Landau Institute for Theoretical Physics, Russian Academy of Sciences, 117940 Moscow, Russia*

(Received 28 April 2011; published 7 July 2011)

The interplay between the superconducting order parameter and elastic fields, which are intimately connected to the very existence of the superconductivity itself, can result in a novel superconducting state: a regular self-organized texture of superconducting islands. We study the formation of these islands in a system of a thin superconducting film coupled elastically to a more rigid substrate and derive the phase diagram below the superconducting critical temperature depending on the elastic coupling constant of both subsystems. The fact that this pattern is a result of the Ginzburg-Landau description of superconductivity indicates that the formation of regular structures may be a common feature of the superconductor transition in the presence of long-range coupling.

DOI: 10.1103/PhysRevB.84.024508 PACS number(s): 74.78.−w, 74.20.De, 74.20.Mn, 74.62.Fj

I. INTRODUCTION

Sixty years ago the volume change accompanying the transition of a superconductor from the normal to the superconducting state was first observed.[1] This discovery–followed by finding the dependence of the superconducting critical temperature T_c on the isotopic mass[2,3] and the change in elastic constants at the transition into the superconducting state[4–6]–guided this line of research crowned eventually by the triumph of the Bardeen-Cooper-Schrieffer (BCS) microscopic theory of superconductivity,[7] which demonstrated an intimate connection between superconductivity and elastic properties of the material.[1,4–6,8] The link between elastic properties and superconductivity[9] has been illustrated by numerous experiments revealing the influence of an external pressure on the critical temperature[10] (see Ref. [11] for an extensive review).

Mechanical stresses, which affect superconductivity, are inherent to thin films attached to a rigid substrate,[12,13] which enforces its lattice spacing on the film. The strains resulting from this elastic coupling lead to a peculiar scenario of the superconducting transition: Upon cooling the film, fluctuation nuclei of the order parameter cause additional strains, which in their turn change the elastic coupling between substrate and film itself leading to a positive feedback between the superconducting order parameter and mechanical stress. The substrate thus mediates an elastic coupling between remote parts of the film, effectively transforming local distortions into long-range elastic coupling, leading to a spatial instability of the superconducting state which eventually forms a periodic hexagonal texture of superconducting islands (see Fig. 1).

Here we study this system of a superconducting thin film coupled elastically to a rigid substrate in the framework of the Ginzburg-Landau theory, taking into account the continuity of the elastic displacement fields and the stress balance equations at the substrate-film interface and film surface.

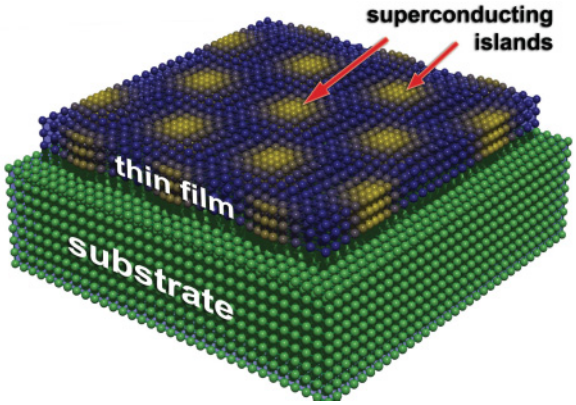

FIG. 1. (Color online) Sketch of a "soft" superconducting film deposited on a rigid substrate. Mechanical stresses induced by the substrate on the film due to mismatch between the lattice constants of the film and of the substrate give rise to an inhomogeneous superconducting state which emerges in the form of a regular array of separated superconducting islands.

The paper is organized as follows: In the following section, Sec. II, the model is introduced, Sec. III describes the process of the island texture formation in detail, and in Sec. IV we construct the phase diagram in the temperature–coupling constant coordinate plane. Finally, we conclude the paper with a discussion our results and its broader implications in Sec. V. In the appendices we present some technical details of our calculations.

II. MODEL

The ground state of a superconducting film coupled to a substrate is derived from the self-consistent solution of coupled Ginzburg-Landau and elasticity theory equations. After integrating out elastic fields one obtains an integro-differential equation for the order parameter of the film which is then solved numerically. In order to improve the accuracy

and reliability of our numerical procedure, we allow our system to evolve in time considering the generalized time-dependent Ginzburg-Landau equation[15–17] (TGLE) instead of a static one. This ensures the rapid convergence to the true ground state in the computational procedure and also allows following, on a qualitative level, the temporal evolution of the superconducting nuclei toward the final equilibrium configuration of the order parameter. We choose a random initial configuration for the order parameter which mimics the random distribution of the superconducting nuclei due to thermal fluctuations expected to form in a homogeneously disordered film upon cooling it down to T_c. However, the final equilibrium island texture does not depend on the particular choice of the initial configuration. The advantage of this approach is that all the richness and complexity of the microscopic elasticity-superconductivity interrelations is accounted for by a phenomenological coupling constant $U_0 = 3\alpha_{\rm L} K(\partial T_c/\partial p)$, where p is the internal pressure, K is the bulk elastic modulus, and $\alpha_{\rm L} = (1/L)(\partial L/\partial T)$ is the linear expansion parameter (with L being the linear dimension of the film). These quantities can be inferred from experiments and contain all information about the electronic degrees of freedom and the lattice excitation spectrum.

The two-dimensional time-dependent Ginzburg-Landau equation describing the order parameter in the film written in dimensionless variables assumes the form

$$\partial_t \psi = \alpha\psi - \beta|\psi|^2\psi + \gamma\nabla^2\psi\,, \qquad (1)$$

where $\psi = \psi(\mathbf{r},t)$ is the complex, dimensionless superconducting order parameter normalized with respect to T_c. The temperature is measured in units of T_c, and the unit of the length is the zero-temperature superconducting coherence length, ξ. We consider the static case where external fields are absent; thus the electromagnetic potentials can be absorbed into the order parameter. The coefficient $\alpha = \alpha_\psi(\mathbf{r})$ is a functional of the order parameter and includes the effects of long-range elastic potentials and temperature T:

$$\alpha_\psi(\mathbf{r}) = \alpha_0[T_c - T] + \int d\mathbf{r}' U(\mathbf{r}-\mathbf{r}')|\psi(\mathbf{r}',t)|^2\,, \qquad (2)$$

where $U(\mathbf{r}-\mathbf{r}')$ is the nonlocal kernel generated by elasticity interactions which is obtained by solving the elastic continuity equations at the interfaces (a more detailed derivation of this expression can be found in Appendix A).

In general, the TGLE without long-range potential has stable homogeneous solutions in the form $\psi = \psi_0 \exp(\imath\,\mathbf{k}\cdot\mathbf{r})$, with $\mathbf{k}$ being a certain constant wave vector [for $T < T_c$, $|\psi_0|^2 = \beta^{-1}(\alpha - \gamma k^2)$, and $\psi = 0$ for $T > T_c$]. Even if a long-range potential is present, the stability of these solutions is only destroyed under certain conditions which can be found by linear stability analysis, which we will discuss in Sec. IV.

Equation (1) is solved on a fine discrete grid by the numerical integration in real and Fourier spaces (*quasi-spectral split-step method*; see Appendix B). For all numerical solutions presented in the following, we use periodic boundary conditions and $N = 512^2$ grid points for a system of size $L^2 = (200\xi)^2$ and film thickness $d = 0.8\xi$. We take into account the full non-local elastic potential. The elastic parameters entering the interaction kernel are $\mu^{(s)} = 0.5$, $\mu^{(p)} = 5.0$ (shear moduli), and $\nu^{(s,p)}/(1-2\nu^{(s,p)}) = 1.6$ (modified Poisson numbers); see also Appendix C for the complete expression. The constant GL parameters are $\alpha_0 = 4.37$, $\beta = 1/2$, and $\gamma = 0.01$.

III. ISLAND FORMATION

In the absence of elastic interactions due to the connection to a substrate, a standard equilibrium solution of the conventional TGLE equation is a spatially uniform order parameter $\psi = \psi_0$ describing a homogeneous superconducting state at $T < T_c$, and $\psi = 0$ for $T > T_c$. The non-local elastic interaction, $U(\mathbf{r}-\mathbf{r}')$, coupling the values of the superconducting order parameter at different points $\mathbf{r}$ and $\mathbf{r}'$ of the film distorts ψ_0 and can give rise to an instability of the uniform solution resulting in the formation of a regular island texture for certain values of the elastic parameters. In this section we present the results of the numerical solution of Eq. (1) in Figs. 2 and 3, using the temperature $T = 0.8T_c$ and the coupling constant $U_0/U_c = 2.23$, where U_c is the critical value of U_0 above which islands appear at zero temperature (see Sec. IV).

In Fig. 2 we present sequential frames of the temporal evolution of the spatial distribution of the amplitude of the order parameter, framing the figure. To quantify the temporal development we introduce the structural correlation function $\mathcal{C}(t)$ shown in the center of the figure. The lower central panel of Fig. 2 shows the final regular hexagonal texture of the amplitude of the order parameter, with $\mathcal{C}(t) = \mathcal{N}^{-1}\sum_k |\psi_k|^2$, where ψ_k denote the Fourier components of the order parameter, and the normalization factor $\mathcal{N}$ is chosen such that $\mathcal{C} = 1$ for $t \to \infty$, when the island texture is fully periodic.

The time is measured in the units of the Ginzburg-Landau time $\tau_{\rm GL}$, with $\tau_{\rm GL} = \pi\hbar/[8k_{\rm B}(T_c - T)]$. Starting from a random order parameter configuration, the system evolves through three clearly distinguishable major stages, reflected by $\mathcal{C}(t)$: (i) an initial amplification of small fluctuations and emergence of an amorphous structure of islands; (ii) the appearance of a polycrystalline configuration of well-separated superconducting islands; and (iii) a slow relaxation of the polycrystalline structure to a regular island lattice, see Fig. 2. Note, that the long-range crystalline order will be established on much larger simulation times for the clean case which we study throughout this paper. If one includes quenched disorder the polycrystalline array can be stabilized with characteristic domain sizes depending on the disorder strength.

The first stage is relatively fast: Establishing an amorphous island pattern takes only about $10\tau_{\rm GL}$, while achieving a polycrystalline structure requires a 10 times longer period. In this intermediate time scale $\mathcal{C}(t)$ evolves logarithmically toward the polycrystalline state. In the final stage, for $t > t_p$, see Fig. 2, where the island polycrystal relaxes toward the regular lattice, the correlation function of the modulus of the order parameter ceases to be an indicative characteristic quantity. At the longest time-scales it is rather the temporal development of the spatial distribution of the *phase* of the order parameter that characterizes the evolution of the system. For the chosen material constants the final state is a superconducting state with a uniform phase distribution corresponding to long-ranged phase coherence. Figure 3 shows that the macroscopic phase-coherent state (which appears as a uniformly colored frame) is achieved via the motion and recombination of vortex-antivortex pairs which are initially

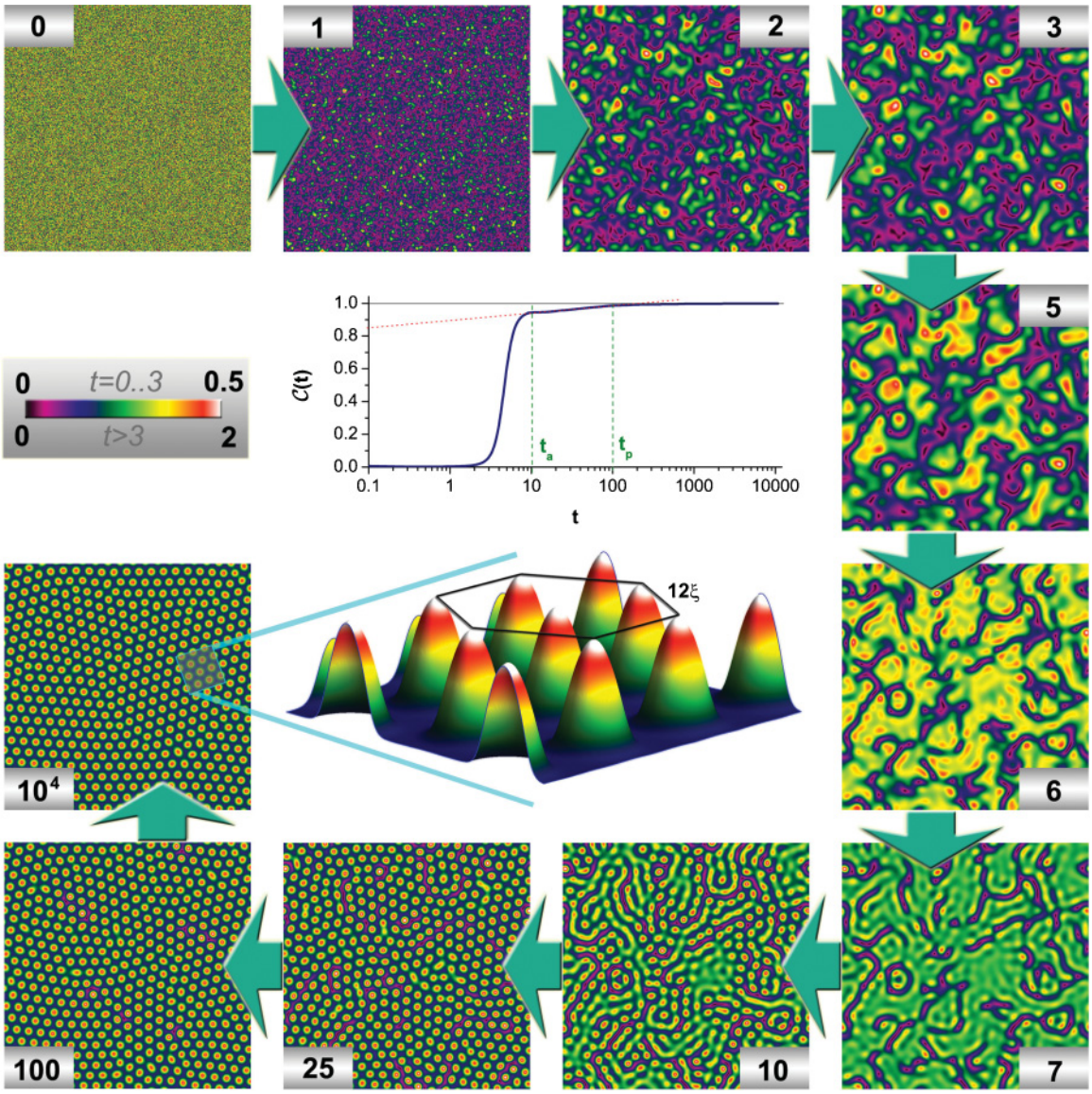

FIG. 2. (Color online) The framing sequence of snapshots shows the temporal evolution of the spatial distribution of the amplitude of the superconducting order parameter. The time is measured in units of the Ginzburg-Landau time, which for temperature $T = 0.8T_c$ can be estimated as $\tau_{\rm GL} \simeq 10^{-11}$ seconds for $T_c \approx 1$ K. The first frame at time $t = 0$ shows an initial random configuration of the order parameter. One can distinguish three stages of the evolution: (i) emergence of an amorphous structure of islands (for $t < t_a \sim 10$); (ii) formation of a polycrystalline islands texture (for $t_a < t < t_p \sim 100$); and (iii) relaxation to a long-range ordered island lattice (for $t > 10^4$). The color bar for the amplitude of the order parameter is presented beneath the initial frame (note the change of the scale for $t > 3$). The upper part of the central panel shows the time evolution of the normalized order parameter correlation function, $\mathcal{C}(t) = \mathcal{N}^{-1} \sum_k |\psi_k|^2$, vs t on a logarithmic scale (ψ_k denote the Fourier components of the order parameter and the normalization factor $\mathcal{N}$ is chosen such that $\mathcal{C} = 1$ when the island texture is fully periodic). At intermediate times between t_a and t_p the correlation function shows transient logarithmic behavior (highlighted by the straight line) and exhibits for $t > t_p$ a slow convergence to unity. The lower part shows a perspective view of the height profile of the amplitude of the order parameter corresponding to a small region of the perfect lattice appearing at the final stage of solution of the TGLE equation. The simulations were done with the coupling constant of $U_0 = 2.23U_c$ and a thickness of the film of 0.8ξ, where ξ is the superconducting coherence length at zero temperature. Defining an "island" as an area within which the amplitude of the order parameter exceeds half of its maximal value, we find their size to be about 2.5ξ and the distance between the centers of the islands to be 12ξ.

present *en masse* in the system due to coalescence of the independent superconducting nuclei in the first stage of the order parameter evolution. The vortex-antivortex pairs are clearly displayed by the "phase-cut" lines that appear as sharp color jumps from black to white. In the same time interval one distinguishes a well pronounced hexagon substructure which shows that different islands have different phases. The global phase coherence and therefore the superconducting state get established by the time of order $10^3\tau_{\rm GL}$, which is by an order of magnitude longer than the time for establishing a robust distribution of the amplitude of the order parameter. We emphasize that our considerations refer to the region below not only

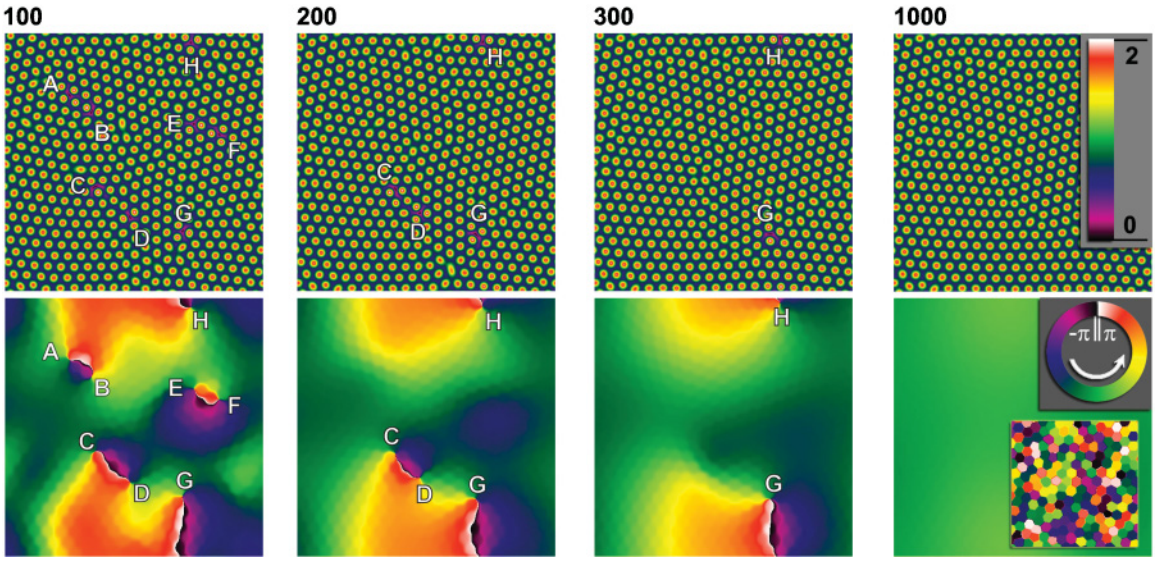

FIG. 3. (Color online) Four sequential snapshots of the amplitude and phase of the order parameter taken at times 100, 200, 300, and 1000 measured in units of $\tau_{\rm GL}$ are presented (the same values of the system parameters as in Fig. 2 were used). The first three frames correspond to nonequilibrium states characterized by an inhomogeneous phase distribution; in this stage the formation of a regular texture of the order parameter amplitude goes along with the recombination of vortex-antivortex pairs. The first frame displays four sets of vortex-antivortex pairs with the end points A-B, C-D, E-F, and G-H. In the corresponding phase frames these end points confine the line of 2π phase jumps visible as sharp color change from white to black (the periodic boundary conditions were used, such that the line G-H goes over the upper and lower edges of the frame). The phase cut lines A-B and E-F disappear at $t = 200$, and at $t = 300$ only the G-H line remains. In the nonequilibrium states, the hexagon-like structure of the phase distribution, reflecting that on the way to equilibrium the phase at the islands is different, is clearly distinguishable (each hexagon represents the phase of an island). At $t = 1000$ the phase becomes homogeneous across the sample and a global phase-coherent superconducting state is established. However, for a different set of parameters the phase equilibration might be very slow or even stopped in the presence of impurities or dissipation, resulting in a random pattern of phases for each island, shown in the inset of the last phase frame.

the superconductor transition temperature T_c, but also well below the Berezinskii-Kosterlitz-Thouless (BKT) transition temperature, $T_{\rm BKT} \lesssim T_c$ [remember that $(T_c - T_{\rm BKT})/T_c \ll 1$], where thermal fluctuations are not relevant. At $T < T_{\rm BKT}$ free vortex-antivortex pairs generated by thermal fluctuations are exponentially rare. Taking into account also that the spatial inhomogeneity brought by these vortices is averaged out on long times scales, one justly concludes that thermally excited vortex-antivortex pairs would not influence the nature of the island texture ground state.

It is important that, while being a general phenomenon, the formation of an island texture requires the elastic coupling to be strong enough. Namely, the texture appears under the condition that the coupling constant U_0 exceeds some temperature-dependent critical value $U_c(T)$. The function $U_c(T)$ is determined by means of linear stability analysis of the TGLE.

IV. PHASE DIAGRAM

The linear stability of the homogeneous solution $\psi = \psi_0$ of the GL equation is examined by expanding the order parameter around ψ_0. After the expansion and the corresponding Fourier transformation, we find that the stability is controlled by the behavior of the function (as $\psi \sim e^{S(q)t}\psi_0$)

$$S(q) = [U_0\mathcal{K}(q) - 1](1 - T/T_c) - \gamma q^2/c\,, \qquad (3)$$

with $c = 8\pi^2/[7\zeta(3)] \approx 9.38$. The instability occurs in the range of parameters where $S(q) > 0$. The behavior of $S(q)$ is determined by that of the elastic kernel $\mathcal{K}(q)$, which is related to the Fourier transform of $U(r)$ as $\hat{U}(q) = U_0\mathcal{K}(q)$.

A plot, illustrating the behavior of $\mathcal{K}(q)$ for two exemplary thicknesses and different elastic constants, is presented in Fig. 4(a). In general, the kernel $\mathcal{K}(q = 0) = 0$, $\mathcal{K}(q \to \infty) = 1/3$, and achieves its maximum value $\mathcal{K}_{\rm M}$ at some $q = q_{\rm M}$. Therefore, $S(q = 0) < 0$ (for $T < T_c$) and $S(q) \to -\infty$ for $q \to \infty$. If $S(q)$ changes its sign at intermediate q the homogeneous solution becomes unstable, see Fig. 4(b). The onset of instability is marked by the values of the parameters at which the maximum of $S(q)$ first touches the q axis. Thus the condition for the island state to form is $(U_0\mathcal{K}_{\rm M} - 1)(1 - T) - \gamma q_{\rm M}^2/c \geqslant 0$. This implies that the coupling constant U_0 should exceed some temperature dependent critical value $U_c(T)$. The function $U_c(T)$ is determined by the form of $S(q)$ given as follows: As can be seen from Fig. 4(b), $S(q)$ can have a positive maximum at some intermediate q; then $U_c(T)$ is the lowest possible value of U_0 satisfying the equation $S(q) = 0$ for a given temperature. We define $U_c \equiv U_c(0)$. This gives $U_c(T) = \mathcal{K}_{\rm M}^{-1} + (\gamma q_{\rm M}^2/c\mathcal{K}_{\rm M})(1 - T/T_c)^{-1}$. The lowest bound for the coupling constant U_c, at which the homogeneous state becomes unstable and the island texture appears, is $U_c = (\gamma q_{\rm M}^2/c + 1)/\mathcal{K}_{\rm M}$. Taking into account the limitations on the values of the material parameters entering the elastic kernel $\mathcal{K}(q)$, one finds that the critical values for U_c are confined to the interval $1.5 \lesssim U_c \lesssim 2$ (corresponding to the observation that

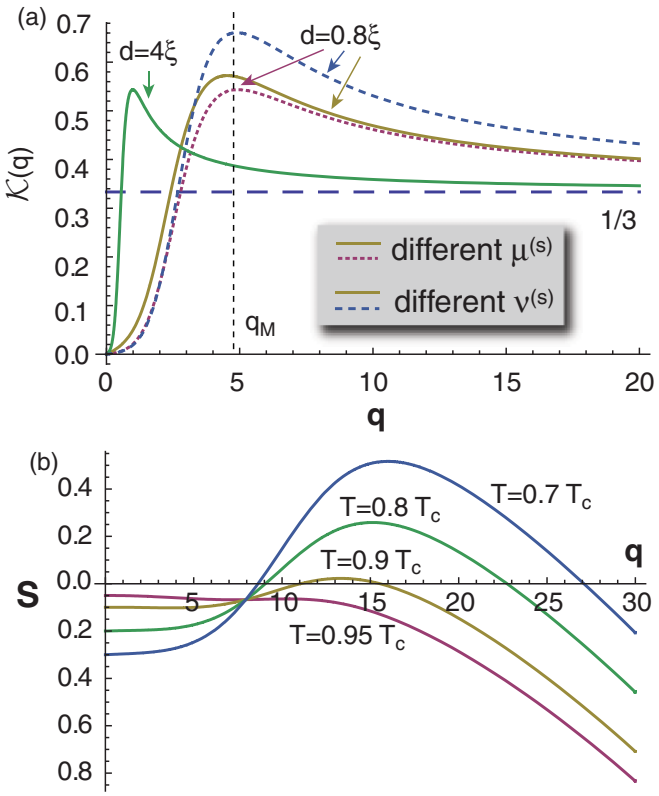

FIG. 4. (Color online) (a) Plot of the elastic kernel $\mathcal{K}(q)$ for different elastic parameters: The graph with maximum close to $q = 0$ [solid, green] is plotted for a thicker film of $d = 4\xi$, the other three for $d = 0.8\xi$. We kept $\mu^{(p)} = 5$, $\sigma_0 = 1.25$, and $\nu^{(p)} = 1.6$ fixed. The three curves with maximum near $q \approx 5$ have $\mu^{(s)} = 0.5$ [dotted, red], $\mu^{(s)} = 2$ [solid, dark yellow] (both $\nu^{(s)} = 1.6$), and $\nu^{(s)} = 1.7$ [dashed, blue] (with $\mu^{(s)} = 0.5$) for the lowest to the highest of these graphs. These graphs demonstrate the weak dependence of $\mathcal{K}(q)$ on different thicknesses d (solid curves), different shear modulus $\mu^{(s)}$ (dotted and solid), and different Poisson number $\nu^{(s)}$ (dashed and solid). (b) Plot of the stability function $S(q)$ with elastic parameters chosen as described in the text for different temperatures and $U_0 = 2.6U_c$ (cf. inset of Fig. 5).

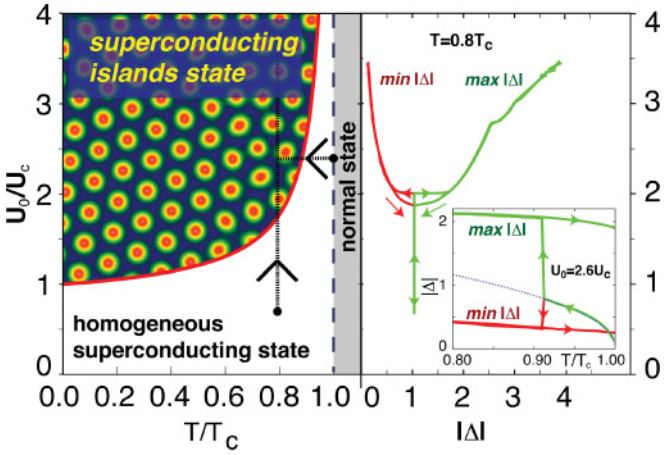

FIG. 5. (Color online) Left panel: The phases in the temperature T-coupling constant U_0 plane. Above T_c the film is in the normal state, whereas below T_c the film can be either a homogeneous superconductor or a textured superconductor consisting of isolated islands. The boundary is determined by the stability condition of the TGLE (see text). Right panel: The amplitude of the order parameter Δ vs coupling constant U_0. The onset of the island texture (crossing the phase boundary) is marked by the bifurcation point where $\Delta_{\max}$ and $\Delta_{\min}$ start to diverge. The observed hysteretic behavior indicates that the formation of the island texture occurs via a first-order transition. The path of change of U_0 is indicated by the vertical arrow in the left panel. The inset in the right panel shows the hysteretic effect corresponding sweeping temperature at fixed $U_0 = 2.6U_c$, first from T_c down to $0.8T_c$, and then heating up (the process shown by the horizontal dotted line in the left panel). The island structure persists even upon heating the system above T_c of the film material, due to the increased local T_c within the islands. The dotted line indicates the usual $\sqrt{1 - T/T_c}$ behavior of the order parameter without elastic interactions.

the values of $\mathcal{K}_M$ are restricted to the interval $0.5 \lesssim \mathcal{K}_M \lesssim 0.7$ and $\gamma q_M^2/c \ll 1$ for a typical film thickness of order ξ). This implies that those are U_0, i.e., $\partial T_c/\partial p$, K, and α_L (see Appendix D for a table with bulk values for comparison), that determine whether the island structure can be realized in a given material.

The resulting phase diagram in reduced T/T_c-U_0/U_c coordinates for the chosen system parameters is shown in the left panel of Fig. 5. The right panel of Fig. 5 shows the behavior of the amplitude of the order parameter $|\Delta|$ at the isotherm $T = 0.8T_c$ as function of the coupling constant U_0. From an initial coupling constant $U_0 < U_c$ and random distribution of the order parameter the system evolves until a stationary distribution of Δ is achieved. After that U_0 is increased and the system evolves again until a new stationary state is achieved (adiabatic increase), and so forth. Upon crossing the phase boundary a bifurcation in the $|\Delta(U_0)|$ dependence corresponding to the island formation occurs and a *finite* difference between the maximal and minimal values of the amplitude of the order parameter appears. On the descending part of the cycle, $|\Delta_{\min}(U_0)|$ and $|\Delta_{\max}(U_0)|$ merge at smaller value of U_0 closer to the phase boundary, i.e., at smaller U_0. The change of U_0 is indicated by the vertical arrow in the left panel of Fig. 5. Shown in the right panel inset is the hysteretic behavior of the order parameter corresponding to sweeping the temperature across the phase transition line. The protocol is nearly the same as for the coupling constant variation scheme; the temperature is first decreased from $T = T_c$ down to $T = 0.8T_c$ and then increased back at the fixed coupling constant $U_0 = 2.6U_c$. The temperature sweeping is indicated by the horizontal arrow in the left panel of Fig. 5. Note that the island structure persists even as the system is heated above T_c; this is the manifestation of the positive feedback between the superconductivity and elasticity giving rise to a local increase in superconducting transition temperature within the islands. The observed hysteretic behavior illustrates that the transition to the island texture states is of the first order. We expect that this transition remains of first order even for small values of quenched disorder in analogy with the Abrikosov vortex lattice, which turns into a *vortex glass* only at sufficiently strong disorder strengths and the transition becomes of second order. However, the inclusion of an additional disorder axis in the phase diagram is beyond the scope of this work and will be subject of further studies.

V. DISCUSSION AND CONCLUSIONS

Pattern formation, in particular, the spontaneous emergence of electronic textures due to the existence of competing states, is ubiquitous in nature and is found in a wealth of complex systems and physical phenomena ranging from magnetism, superconductivity, and superfluidity to liquid crystals and dynamics of biological systems.[14,15] A profound example of a regular electronic texture is the Abrikosov lattice,[18] a periodic array of filaments of the normal phase arising as a result of the penetration of the magnetic field into a type II superconductor. We have shown above that in the general experimental situation of a superconducting film attached elastically to a rigid substrate, superconductivity can nucleate in the form of a regular array of superconducting islands. A quantitative description of the emerging texture is achieved within the framework of a general approach to pattern formation based on the TGLE. On a technical level, taking into our consideration the coupling of the superconducting order parameter to the elastic stress arising due to a mismatch between the substrate and film lattices, and then integrating out the elastic degrees of freedom, gives rise to the non-local term in the Ginzburg-Landau functional. This, in its turn, results in the instability of the homogeneous superconducting state, provided the coupling constant exceeds some the temperature-dependent critical value. We would like to emphasize here that this texture of superconducting islands is dual to the Abrikosov vortex state, although it emerges in the absence of a magnetic field. In our case the role of the magnetic field is taken by the stress fields (and instead of Maxwell equations that can be solved self-consistently with the GL equation to produce the Abrikosov lattice, we have elasticity equations). The criterion for the formation of the island texture is derived by virtue of linear stability analysis which relates the onset of instability with respect to the island texture formation to the behavior of the linear growth rate function $S(q)$, Eq. (3). This function starts changing its sign at the instability line leading to the phase diagram presented in the previous section. A remarkable effect of the effective long-range interaction (resulting in our case from the elasticity equations) is that the transition into the island state is of *first order*. This transition occurs below T_c upon lowering the temperature. However, with increasing temperature, the island state remains stable even above the critical temperature, reflected by the hysteretic behavior of the order parameter values inside and outside the islands (Fig. 5).

It is noteworthy that it is the non-locality in the Ginzburg-Landau functional that results in the texture formation irrespectively of its specific origin. We expect that the interplay of strong disorder with long-range Coulomb interaction near the disorder-driven superconductor-insulator transition (SIT) can also result in a non-local coupling which eventually can generate an island-like texture.[19] We, however, defer the microscopic derivation of the proper functional to a forthcoming publication. Concerning the role of Coulomb interactions, it was argued in a recent work[20] that Coulomb effects can transform the SIT into a first-order transition. This would imply the possibility of an electronic phase separation and a probable formation of a regular array of electronic islands in the course of the SIT in agreement with the conjecture of Refs. 21 and 22.

Another important comment is that the island texture appears in clean films and remains stable in the presence of weak disorder. Moreover, weak disorder as well as thermal fluctuations favor the initial formation of the island state promoting nucleation seeds for local lattice deformations. Yet, we reiterate that the island texture is an inherent property of superconductivity coupled to the elastic field and emerges as a result of the instability of the initially homogeneous order parameter distribution. In this respect the observed regular island structure has to be distinguished from the disorder-induced spatially inhomogeneous distribution of the order parameter in Refs. 23–26.

Finally, the observed island texture is, in fact, an array of granules of a "good" superconductor immersed into a sea of a "bad" one (characterized by the depressed amplitude of the order parameter). This texture can be viewed as a self-assembled array of nanoscale Josephson junctions, which may appear in either the superconducting or the insulating state depending on the relative strength of the Josephson coupling.[28–30] In our simulations, where thermal and quantum fluctuations are absent, the Josephson coupling, however weak, eventually establishes a global phase coherence, i.e., global superconductivity. In reality, fluctuations, dissipation, and disorder can break down this phase uniformity and drive the array into an insulating state. The intermediate stages of the evolution of phase distribution in our simulations (see Fig. 3), which correspond to the temporal scales on which a global phase coherence is not yet established, can therefore represent the final states of the real systems—in particular, for larger coupling constants U_0, phase distributions like the hexagonal "mosaic" in the inset of the last phase frame of Fig. 3 can prevail. Thus our finding that the transition into the superconducting state of two-dimensional superconductors elastically tied to a substrate can occur via the formation of a nanoscale superconducting island texture offers a possible scenario for a superconductor-to-insulator transition observed in various thin superconducting films.[27,31–38]

ACKNOWLEDGMENTS

We thank Yuri Galperin and David Hinks for useful discussions. This work was supported by the US Department of Energy Office of Science, Division of Materials Science and Engineering, under the Contract No. DE-AC02-06CH11357. The work of T.B. and N.C. was partly supported by the Program "Quantum Physics of Condensed Matter" of the Russian Academy of Sciences, and by the Russian Foundation for Basic Research (Grants No. 09-02-01205 and 09-02-12206). N.C. acknowledges support by the Materials Theory Institute at ANL.

APPENDIX A: CONSTRUCTION OF THE ELASTIC INTERACTION POTENTIAL U

Here we derive $U(\mathbf{r})$ for the problem of a thin superconducting elastic film coupled to a rigid substrate with different elastic properties and lattice mismatch. In the following, we use the superscripts (s) for all quantities related to the film, and (p) for the substrate. Both materials are described by the

three-dimensional displacement fields $\mathbf{u}^{(s)}/\mathbf{u}^{(p)}$. We start our consideration using a plane-wave ansatz for these fields:

$$u_x^{(s)} = e^{\imath q_x x+\imath q_y y}\left(e^{q_z z}A_{1,x} + A_{2,x}e^{-q_z z} + u_{0,x}^{(s)}\right),$$
$$u_y^{(s)} = e^{\imath q_x x+\imath q_y y}\left(e^{q_z z}A_{1,y} + A_{2,y}e^{-q_z z} + u_{0,y}^{(s)}\right),$$
$$u_z^{(s)} = e^{\imath q_x x+\imath q_y y}\left(e^{q_z z}A_{1,z} + A_{2,z}e^{-q_z z}\right),$$
$$u_x^{(p)} = C_x e^{q_z z+\imath q_x x+\imath q_y y}, \quad u_y^{(p)} = C_y e^{q_z z+\imath q_x x+\imath q_y y},$$
$$u_z^{(p)} = C_z e^{q_z z+\imath q_x x+\imath q_y y},$$

where the misfit strain on the film is captured by the real exponential terms of the film in the z direction. $u_{0,x}^{(s)}$ and $u_{0,y}^{(s)}$ are special solutions of the two-dimensional problem due to superconductivity, which we will discuss later. In order to determine the nine free parameters C_i, $A_{1,i}$, and $A_{2,i}$ we need nine equations. First, we consider the interface film vacuum at $z = d$, where d is the thickness of the film. The stress boundary condition for a flat surface demands $\sigma_{xz} = \sigma_{yz} = \sigma_{zz} = 0$. So, for the film we get from Hooke's law

$$\sigma_{xz}^{(s)} = \mu^{(s)}\left(\partial_z u_x^{(s)} + (1-2\sigma_0)\partial_x u_z^{(s)}\right),$$
$$\sigma_{yz}^{(s)} = \mu^{(s)}\left(\partial_z u_y^{(s)} + (1-2\sigma_0)\partial_y u_z^{(s)}\right),$$
$$\sigma_{zz}^{(s)} = 2\mu^{(s)}\left[(1+\nu^{(s)})\partial_z u_z^{(s)} + \nu^{(s)}\left(\partial_x u_x^{(s)} + \partial_y u_y^{(s)}\right)\right],$$

where the effect of a lattice mismatch of both materials is captured by the σ_0 term which takes into account small deformations of the surface in z-direction. In general, the lattice constants of both materials are different; i.e., the misfit parameter $\eta = (a^{(s)} - a^{(p)})/a^{(p)}$ is nonzero, where $a^{(s)}$ and $a^{(p)}$ are the lattice constants of the film and substrate, respectively. This lattice mismatch leads to a compression of the film lattice at the interface, such that the lattice spacings match there. We note that this description not only applies to crystalline structures but also for amorphous materials, where the "lattice" constants are averaged quantities.

The coefficients $\mu^{(s)}$ and $\nu^{(s)}$ are the shear modulus and the modified Poisson number of the film [$\nu^{(s)} = \tilde{\nu}^{(s)}/(1-2\tilde{\nu}^{(s)})$, where $\tilde{\nu}^{(s)}$ is the Poisson number]. In the following we use the fact that all interface equations are independent of the x and y coordinates in first order of the interface deformation and set $x = y = 0$. Therefore, the first three of the nine equations are

$$\sigma_{iz}^{(s)}(0,0,d) = 0 \text{ for } i = x,y,z\,. \tag{A1}$$

Next, we consider the interface between film and substrate at $z = 0$, for which we also need the expressions for the stress tensor elements:

$$\sigma_{xz}^{(p)} = \mu^{(p)}\left(\partial_z u_x^{(p)} + \partial_x u_z^{(p)}\right),$$
$$\sigma_{yz}^{(p)} = \mu^{(p)}\left(\partial_z u_y^{(p)} + \partial_y u_z^{(p)}\right),$$
$$\sigma_{zz}^{(p)} = 2\mu^{(p)}\left[(1+\nu^{(p)})\partial_z u_z^{(p)} + \nu^{(p)}\left(\partial_x u_x^{(p)} + \partial_y u_y^{(p)}\right)\right].$$

At this interface we need to fulfill six more conditions, where three of them are resulting from the stress balance,

$$\sigma_{iz}^{(s)}(0,0,0) = \sigma_{iz}^{(p)}(0,0,0) \text{ for } i = x,y,z,$$

and the last three equations are the continuity equations for the displacement fields,

$$u_i^{(s)}(0,0,0) = u_i^{(p)}(0,0,0) \text{ for } i = x,y,z.$$

These nine equations can now be solved in order obtain the free parameters of our ansatz.

The two special solutions for $u^{(s)}$ in the x and y directions, $u_{0,i}^{(s)}$, already used in the ansatz for the deformation fields of the film, are obtained through solution of the extended stress-strain balance,

$$\beta^{(s)}\Delta\mathbf{u}^{(s)} + \nabla(\nabla\mathbf{u}^{(s)}) = \gamma^{(s)}\nabla|\psi(\mathbf{r})|^2\,, \tag{A2}$$

which takes into account that the system's energy is the sum of the superconducting energy and the mechanical deformation energy. This relation introduces two phenomenological parameters, $\gamma^{(s)}$ and $\beta^{(s)}$, which together define the coupling constant of the elastic interaction and superconductivity which is determined explicitly below. Equation (A2) can be solved and gives

$$u_{0,i}^{(s)} = -\imath\gamma_s\frac{f(q)q_i}{(1+\beta_s)\mathbf{q}^2} \tag{A3}$$

for $i = x,y$.

Using the solutions for all coefficients we find the internal pressure of the film:

$$p^{(s)}(q_x,q_y,q_z) = \frac{1}{3d}\int_0^d dz\left(\partial_x u_x^{(s)} + \partial_y u_y^{(s)} + \partial_z u_z^{(s)}\right). \tag{A4}$$

This expression simplifies to $p^{(s)}(q_z)$ if we use the homogeneous parametrization $q_x = q_z\cos(\theta)$, $q_y = q_z\sin(\theta)$. Due to the special solution for $u^{(s)}$ the pressure $p^{(s)}(q)$ is proportional to $|\psi_q|^2$, where ψ_q are the Fourier components of the order parameter.

Now, we need to consider the connection of elasticity and superconductivity. For that, we first expand T_c in changes of (internal) pressure:

$$T_c(p = p_0 + \Delta p) = T_c(p_0) + \Delta p\frac{\partial T_c(p_0)}{\partial p}. \tag{A5}$$

The pressure change Δp is related to a volume change ΔV as $K = -V\partial p/\partial V$, where K is the bulk modulus. Therefore we can write

$$\Delta p = -K\frac{\Delta V}{V} = -3K\frac{\Delta L}{L} \propto -3K\alpha_{\text{L}}, \tag{A6}$$

where $\Delta L/L$ is the relative length change of the system and α_{L} the linear thermal expansivity of the film.

Using the above result in the pressure-expanded critical temperature, the parameter α in the TGLE obtains thus the non-local form

$$\alpha_\psi(\mathbf{r}) = \alpha_0[T_c - T] + \int d\mathbf{r}' U(\mathbf{r}-\mathbf{r}')|\psi(\mathbf{r}',t)|^2. \tag{A7}$$

We note that T_c could also include spatial variations due to disorder. However, here we consider only the clear case.

We define the scale free elastic kernel

$$\mathcal{K}(q) = \frac{(1+\beta^{(s)})}{\gamma^{(s)}}\frac{p^{(s)}(q)}{|\psi(\mathbf{r})|^2}, \tag{A8}$$

where the explicit form of the elastic kernel is quite involved and given in Appendix C. Finally, we write the Fourier transform of $U(\mathbf{r})$ as $U_0\,\mathcal{K}(q)$, where $U_0 = 3K\Delta\alpha_{\text{L}}[\partial T_c(p_0)/\partial p]$.

APPENDIX B: NUMERICAL REALIZATION

The TGLE equation,

$$\partial_t \psi = \alpha\psi - \beta|\psi|^2\psi + \gamma\nabla^2\psi, \tag{B1}$$

is solved by a quasi-spectral split-step method for periodic boundary conditions on a two-dimensional square grid with grid size of N^2 for a system size L^2. *Split step* means that for each time step the equation is solved partially in real space and partially in Fourier space (the diffusion part).[15] In the first step we calculate

$$\psi_{ij}(t+\Delta t) = e^{\Delta t(\alpha-\beta|\psi_{ij}|^2)}\psi_{ij}(t), \tag{B2}$$

where the non-local part of α is calculated by fast Fourier transformation (FFT) up front.

Then, in the second step, we first Fourier-transform $\psi_{ij}(t+\Delta t)$, apply the diffusion kernel, and transform it back. This way we avoid mostly all complications of the diffusion equation.[15]

For large coupling constants U_0 we also introduced a small higher order term $\propto -\delta|\psi|^4\psi$ in the TGLE to improve the numerical stability, with $\delta = 0.01$. However, this term does not influence the result.

In general the TGLE without long-range potential has only two stable solutions: a homogeneous one and a striped phase. Even if a long-range potential is present, the stability of these two solutions is only destroyed under certain conditions which can be found by the linear stability analysis. For example, a Coulomb potential or even screened Coulomb potential cannot create this kind of instability by itself. At variance, the elastic potential breaks down the stability of the two basic above solutions, provided the parameters are chosen appropriately. Another possible nonlocal potential which destroys the homogeneous/striped solutions is a box potential[39] $U(\mathbf{r}) = U_0\Theta(1-|\mathbf{r}|/a)$.

APPENDIX C: ELASTIC KERNEL AND SIMULATION PARAMETERS

The full expression of the elastic kernel $\mathcal{K}(q)$, depending on the dimensionless material parameters, is given by

$$\begin{aligned}\mathcal{K}(q) = \big\{&\mu_p^2(1+2\nu^{(p)})[dq(1+e^{4dq})\vartheta_s - (e^{4dq}-1)(2\vartheta_s+1)] + dq[e^{4dq}\mu_s\vartheta^{(s)}(2\mu^{(p)}+2\mu^{(p)}\nu^{(p)}\sigma_0 - \mu^{(s)}\vartheta^{(s)})\\
&- \mu^{(s)}\vartheta^{(s)}(\mu^{(s)}\vartheta^{(s)} + 2\mu^{(p)}[1+\nu^{(p)}+\nu^{(s)}-\nu^{(p)}\sigma_0]) - 2e^{2dq}(\mu^{(p)2}[1+2\nu^{(p)}][1+2\nu^{(s)}\sigma_0]\\
&- \mu^{(s)2}\vartheta^{(s)2} - \mu^{(p)}\mu^{(s)}\vartheta^{(s)}(\nu^{(p)}+\nu^{(s)}-2\nu^{(p)}\sigma_0))] + \mu^{(s)}(e^{dq}-1)^2[4\mu^{(s)}\nu^{(s)}(e^{2dq}-1)\vartheta^{(s)}[\sigma_0-1]\\
&+ \mu^{(p)}[1+2\nu^{(s)}(2-2\vartheta^{(s)}-3\sigma_0)+2\nu^{(p)}[2\vartheta^{(s)}+1][\sigma_0-1] - 2e^{dq}(\nu^{(s)}(2\nu^{(p)}[\sigma_0-1]+2\sigma_0-3)-1)\\
&- e^{2dq}(3\vartheta^{(s)}+2+2\nu^{(p)}[\sigma_0-1](\nu^{(s)}[4\sigma_0-2]-1))]] + 4\mu^{(p)2}\nu^{(s)}e^{2dq}[1+2\nu^{(p)}][4\sigma_0-3]\\
&\times \sinh(dq)\big\}/\{3dq\{-\mu^{(s)2}(e^{2dq}-1)^2\vartheta^{(s)2} + 2\mu^{(p)}\mu^{(s)}(e^{2dq}-1)\vartheta^{(s)}(1+\nu^{(p)}+\nu^{(s)}-\nu^{(p)}\sigma_0+e^{2dq}[1+\nu^{(p)}\sigma_0])\\
&+ \mu^{(p)2}(1+2\nu^{(p)})(e^{4dq}\vartheta^{(s)} + 2\nu^{(s)}[\sigma_0-1] - 1 - 2e^{2dq}[1+2\nu^{(s)}\sigma_0])\}\},\end{aligned} \tag{C1}$$

with $\vartheta^{(s)} \equiv 2\nu^{(s)}[\sigma_0-1]-1$, thickness of the film, d, and the elastic parameters: shear modulus, $\mu^{(s,p)}$; deformation stress, σ_0; and modified Poisson numbers, $\nu^{(s,p)}$.

Shown in Fig. 4(a) are plots of $\mathcal{K}(q)$ for different film thicknesses and elastic parameters. For the simulations (cf. evolution of amplitude and phase in Figs. 2 and 3) we used the typical values: $T = 0.8T_c$, $U_0 = 2.23U_c$, $\gamma = 0.01$, $\beta = 0.5$, $d = 0.8\xi$, $\mu^{(s)} = 0.5$, $\mu^{(p)} = 5$ (the substrate is more rigid), $\nu^{(s)} = \nu^{(p)} = 1.6$, $\sigma_0 = 1.25$, $L = 200\xi$ (linear dimension of the system), and $N = 512$ (number of discrete grid points per dimension) [the corresponding plot of $\mathcal{K}(q)$ is given by the dark yellow, solid curve in Fig. 4(a)]. In Fig. 4(a) the elastic kernel is plotted for modified Poisson ratios $\nu^{(s)}$ and $\nu^{(p)}$ taken between 1.5 and 2 (which is the interval restricting the range of possible modified Poisson ratios for all typical materials) and for the relative shear moduli (normalized to the bulk modulus) which are typically confined between 0.5 and 5. The plots of Fig. 4(a) illustrate that both $\mathcal{K}_M$ and q_M do not change much upon varying elastic constants and film thickness.

APPENDIX D: BULK MATERIAL PARAMETERS FOR COMPARISON

As a practical matter, when checking whether the island structure can be realized in a given material, one has to focus on the coupling constant U_0, i.e., on the quantities $\partial T_c/\partial p$, K, and α_L, defining it. Table I presents the material parameters and the corresponding coupling constants for several superconducting

TABLE I. Estimate of the coupling constant $U_0 = 3K\alpha_L\partial T_c/\partial p$ for different materials. The values are given for bulk materials and therefore define only the lower limit for thin films. (a) Data from Ref. 40 for bulk, anisotropic material; (b) from Ref. 41: bulk, $x = 0.074$; (c) from Ref. 42: bulk, organic.

Material	T_{c0} (K)	$\partial T_c/\partial p$ (K/GPa)	α_L (1/K)	K (GPa)	U_0
(a) $YBa_2Cu\text{-}3O_{7-\delta}$	90.9	1.9–2.2 (a,b axis)	$(0.5–1)\times10^{-6}$	200–250	2×10^{-3}
(b) $Ba(Fe_{1-x}Co_x)_2As_2$	21	−26 (c axis)	-11.7×10^{-6}	∼250	∼0.23
(c) κ-$(D_8\text{-ET})_2Cu(NCS)_2$	9	−30 (hydrostatic)	8×10^{-6}	12.2	-10^{-2}

materials. Note that it contains the data for the bulk values of the elastic parameters. At this time, data for elastic properties of thin films which are necessary for calculating the coupling constant are not available.

[1] B. G. Lasarev and A. I. Sudovtsov, Dokl. Akad. Nauk SSSR **69**, 345 (1949).
[2] E. Maxwell, Phys. Rev. **78**, 477 (1950).
[3] C. A. Reynolds, B. Serin, W. H. Wright, and L. B. Nesbitt, Phys. Rev. **78**, 487 (1950).
[4] J. K. Landauer, Phys. Rev. **96**, 296 (1954).
[5] J. L. Olsen, Nature (London) **175**, 37 (1955).
[6] P. Grassmann and J. L. Olsen, Helv. Phys. Acta **28**, 24 (1955).
[7] J. Bardeen, L. N. Cooper, and J. R. Schrieffer, Phys. Rev. **108**, 1175 (1957).
[8] D. Shoenberg, *Superconductivity* (Cambridge University Press, Cambridge, 1952), p. 74.
[9] H. Kronmüller, Phys. Status Solidi **40**, 295 (1970).
[10] B. Lasarev and L. Kan, Zh. Eksp. Teor. Fiz. **14**, 463 (1944).
[11] B. Lorenz and C. W. Chu, in *Frontiers in Superconducting Materials*, edited by Anant V. Narlikar (Springer, Berlin, 2005), p. 459.
[12] S. Qin, J. Kim, Q. Niu, and C. K. Shih, Science **324**, 1314 (2009).
[13] T. Zhang *et al.*, Nature Phys. **6**, 104 (2010).
[14] E. Dagotto, Science **309**, 257 (2005).
[15] I. S. Aranson and L. Kramer, Rev. Mod. Phys. **74**, 99 (2002).
[16] V. L. Ginzburg and L. D. Landau, Zh. Eksp. Teor. Fiz. **20**, 1064 (1950).
[17] N. Kopnin, *Theory of Nonequilibrium Superconductivity*, International Series of Monographs on Physics (Clarendon Press, Oxford, 2000).
[18] A. A. Abrikosov, Zh. Eksp. Teor. Fiz. **32**, 1442 (1957) [Sov. Phys. JETP **5**, 1174 (1957)].
[19] A. Glatz, I. Aranson, V. M. Vinokur, N. M. Chtchelkatchev, and T. I. Baturina, e-print arXiv:0910.0659.
[20] S. V. Syzranov, I. L. Aleiner, B. L. Altshuler, and K. B. Efetov, Phys. Rev. Lett. **105**, 137001 (2010).
[21] M. V. Fistul, V. M. Vinokur, and T. I. Baturina, Phys. Rev. Lett. **100**, 086805 (2008).
[22] V. M. Vinokur, T. I. Baturina, M. V. Fistul, A. Yu. Mironov, M. R. Baklanov, and C. Strunk, Nature (London) **452**, 613 (2008).
[23] A. Ghosal, M. Randeria, and N. Trivedi, Phys. Rev. Lett. **81**, 3940 (1998).
[24] A. Ghosal, M. Randeria, and N. Trivedi, Phys. Rev. B **65**, 014501 (2001).
[25] Y. Dubi, Y. Meir, and Y. Avishai, Nature (London) **449**, 876 (2007).
[26] Y. Imry, M. Strongin, and C. C. Homes, Physica C **468**, 288 (2008).
[27] B. Sacépé, C. Chapelier, T. I. Baturina, V. M. Vinokur, M. R. Baklanov, and M. Sanquer, Phys. Rev. Lett. **101**, 157006 (2008).
[28] J. E. Mooij, B. J. van Wees, L. J. Geerligs, M. Peters, R. Fazio, and G. Schön, Phys. Rev. Lett. **65**, 645 (1990).
[29] R. Fazio and G. Schön, Phys. Rev. B **43**, 5307 (1991).
[30] H. S. J. van der Zant, W. J. Elion, L. J. Geerligs, and J. E. Mooij, Phys. Rev. B **54**, 10081 (1996).
[31] E. Bielejec, J. Ruan, and W. Wu, Phys. Rev. Lett. **87**, 036801 (2001).
[32] E. Bielejec, J. Ruan, and W. Wu, Phys. Rev. B **63**, 100502(R) (2001).
[33] G. Sambandamurthy, L. W. Engel, A. Johansson, and D. Shahar, Phys. Rev. Lett. **92**, 107005 (2004).
[34] G. Sambandamurthy, L. W. Engel, A. Johansson, E. Peled, and D. Shahar, Phys. Rev. Lett. **94**, 017003 (2005).
[35] N. Hadacek, M. Sanquer, and J-C. Villégier, Phys. Rev. B **69**, 024505 (2004).
[36] T. I. Baturina, C. Strunk, M. R. Baklanov, and A. Satta, Phys. Rev. Lett. **98**, 127003 (2007).
[37] T. I. Baturina, A. Yu. Mironov, V. M. Vinokur, M. R. Baklanov, and C. Strunk, Phys. Rev. Lett. **99**, 257003 (2007).
[38] T. I. Baturina, A. Bilušić, A. Yu. Mironov, V. M. Vinokur, M. R. Baklanov, and C. Strunk, Physica C **468**, 316 (2008).
[39] Y. Pomeau and S. Rica, Phys. Rev. Lett. **72**, 2426 (1994).
[40] C. Meingast, O. Kraut, T. Wolf, H. Wühl, A. Erb, and G. Müller-Vogt, Phys. Rev. Lett. **67**, 1634 (1991).
[41] S. L. Bud'ko, N. Ni, S. Nandi, G. M. Schmiedeshoff, and P. C. Canfield, Phys. Rev. B **79**, 054525 (2009).
[42] J. Müller *et al.*, Phys. Rev. B **61**, 11739 (2000).